# Grazing-incidence x-ray-scattering study of step-step correlations on Si(001) surfaces

G. Renaud,* P. H. Fuoss, J. Bevk, and B. S. Freer
*AT&T Bell Laboratories, Murray Hill, New Jersey 07974*
(Received 19 July 1991; revised manuscript received 12 November 1991)

In this work, x-ray scattering was used to study regularly spaced steps on Si(001) surfaces. Staircases of steps were obtained after molecular-beam epitaxy of silicon onto atomically flat Si(001) surfaces with a small residual miscut ($\sim 0.05°$), and subsequent annealing at high temperature. Crystal-truncation-rod intensities are shown to be strongly affected by the macroscopic miscut. Detailed statistical information, such as the average terrace width and terrace-width disorder, were derived by analysis of the truncation-rod intensity distribution. The excellent resolution of the synchrotron experiment enabled us to show that, in some cases, the width of the diffraction peaks is very small, which is shown to arise from long-range correlations between successive terrace widths. A simple model is derived to analyze the peak intensity distribution without relying on the common assumption of statistical independence between neighboring terrace widths. By comparison with an unannealed sample, we show that annealing at high temperature favors the step ordering.

## I. INTRODUCTION

Steps strongly affect several fundamental properties of surfaces, including electronic surface states, sticking coefficient, and surface reconstructions.[1] They are involved in surface critical phenomena and roughening transitions and play a dominant role in the processes of thin-film epitaxial growth.[2] Although crystal-growth morphology and kinetics are strongly affected by the substrate-surface step topography, these steps are, in turn, strongly dependent on the precise surface-preparation procedures. In particular, the step height and step ordering caused by molecular-beam-epitaxy (MBE) growth may differ from the equilibrium state. Recent scanning-tunneling-microscopy (STM) studies of Si(001) surfaces grown by MBE (Ref. 3) have dealt with the preparation of single-domain dimer-reconstructed surfaces, where the steps between adjacent terraces are even number of monolayers high, by selective growth at one of the two nonequivalent types of uneven-height step edges.[4] Biatomic steps have been observed mostly on vicinal surfaces, a fact that is well understood by present theories.[1] However, several recent studies on well-oriented substrates have shown, after annealing at $\sim 1273$ K, the existence of a single-domain surface implying the presence of bilayer steps.[5] The orientation of the step edges with respect to the [110] and [$1\bar{1}0$] directions is believed to play a role in this latter case.[1,6] Determination of the size distribution of terraces is a prerequisite to any quantitative investigation of the fundamental physical processes involved in stepped surfaces.

We present here grazing-incidence x-ray-scattering (GIXS) studies of regularly spaced steps on epitaxially grown Si(001) surfaces. The sample preparation will be described first, followed by a brief description of the technique and of the experimental conditions. The magnitude and in-plane orientation of the small residual miscut are next precisely determined. A detailed analysis of the mean terrace width and terrace-width disorder is performed, and the existence, in some cases, of long-range terrace-width correlations is shown. The effects of high-temperature annealing, oxidation, and residual stress are illustrated by comparing several samples.

## II. EXPERIMENTAL DESCRIPTION AND PARAMETERS

The initial 4-in. silicon wafers were precisely cut parallel (to within $\sim 0.05°$) to the (001) atomic planes, and prepared by a free-floating polishing process.[7] Pieces measuring $4\times4$ cm$^2$ were cut from these wafers and mounted in a MBE chamber. The preparation conditions for the three samples described in this paper are summarized in Table I. After heating to 1173 K to desorb the oxide obtained by standard procedures, a buffer layer of 2500 Å of silicon was grown on them by MBE at 873 or 1023 K to enhance the surface perfection. Two samples were then annealed at high temperature for 20 min. Such an anneal has recently been found to yield nearly single-domain surfaces, even on samples with a small miscut.[5] Indeed, on sample 1, the $2\times1$ fractional-order reflections of the reflection high-energy electron-diffraction (RHEED) pattern corresponding to the dimer reconstruction[8] were much more intense than the $1\times2$ reflections at that stage of the process. We conclude that bilayer steps (or pairs of monolayer-high steps very close to each other) were present on a large area of sample 1. Sample 3 was not annealed at high temperature, but instead cooled down directly to room temperature. On samples 2 and 3 the resulting RHEED pattern clearly displayed both types of dimer-reconstruction peaks with comparable intensities, which implies that a large number of monolayer-high steps were present. The specimens were next oxidized in dry oxygen at atmospheric pressure for 4 h at room temperature in the MBE chamber load-lock system, and then oxidized respectively for another 8 h (samples 1 and 2) and another week (sample 3) at room temperature in air.

TABLE I. Summary of the sample-preparation conditions. Also shown are the different parameters relative to the miscut determined in this study: in-plane orientation, value of the miscut, and mean terrace width.

| Sample No. | Growth temperature (K) | Anneal at high $T$ | RHEED symmetry | Oxidation in air | Miscut $m$ (deg) | Miscut orientation $\phi$ (deg) | Mean unit width $W$ (Å) |
|---|---|---|---|---|---|---|---|
| 1 | 873 | YES (1273 K) | 2×1 | 8 h | 0.047 | 16.5 | 3300 |
| 2 | 1023 | YES (1223 K) | 2×1 and 1×2 | 8 h | 0.031 | 46 | 5000 |
| 3 | 873 | NO | 2×1 and 1×2 | 1 week | 0.060 | 38 | 2600 |

The GIXS measurements[9] were performed at beam line X16A at the National Synchrotron Light Source at Brookhaven National Laboratory, which delivered a monochromatic (8925-eV) photon flux of $\sim 5\times 10^{10}$ photons/sec mm$^2$. The samples were mounted in an ultrahigh-vacuum (UHV) chamber coupled to a 5-circle diffractometer designed specifically for GIXS measurements.[10] The incident and scattered wave vectors were set slightly above the critical angle for total external reflection.

Accurate knowledge of the in-plane resolution function is essential to the analysis of the data described in the following. We estimate the shape of the resolution function for a given scattering configuration from Ewald's construction (Fig. 1). The resolution function is approximated by a highly asymmetric parallelepiped, which is tilted by an angle $(2\theta)/2$ with respect to the momentum-transfer direction. The length $\Delta q_L$ and width $\Delta q_W$ of the resolution function are related to the incoming, $\Delta\alpha$, and outgoing, $\Delta\beta$, beam divergences by $\Delta q_L=(2\pi/\lambda)\Delta\beta \sim 2\times 10^{-2}$ Å$^{-1}$ and $\Delta q_W=(2\pi/\lambda)\Delta\alpha\sim 6\times 10^{-4}$ Å$^{-1}$, where $\lambda$ is the wavelength of the monochromatic x-ray beam. The longitudinal resolution is given by $\Delta q_{\parallel}=\Delta q_L \cos[1/2(2\theta)]$, whereas the transverse effective resolution $\Delta q_T=2\Delta q_W \sin[1/2(2\theta)]$ if the peak width is comparable to $\Delta q_W$. In Fig. 1 the angle between $\mathbf{q}$ and the resolution function is negative, which was checked by mapping the intensity measured around the bulk $(2\bar{2}0)$ reflection. The experimental width and length were consistent with those calculated above. The width of this resolution function varies according to the measurement's location in reciprocal space. From the widths of the {220} peaks and those of {110} peaks to be described later, the coherence length of the x-ray beam is $\sim 1.6$ $\mu$m at {220} reflections and $\sim 4.6$ $\mu$m at {110} reflections.

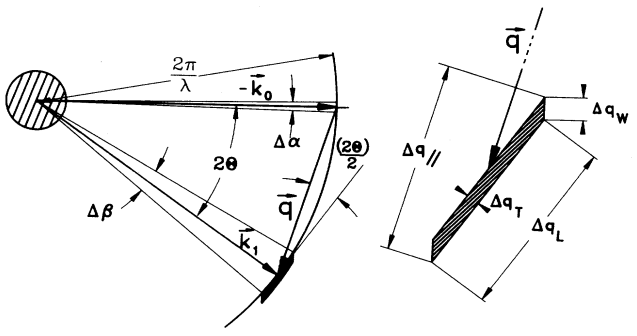


FIG. 1. Ewald's construction for the grazing-incidence x-ray-scattering configuration. The scattering plane, which is close to the surface plane, is represented. $2\theta$ is the in-plane angle between the incident beam, of wave vector $\mathbf{k}_0$, and the scattered beam, of wave vector $\mathbf{k}_1$; $\mathbf{q}$ is the scattering vector (or momentum transfer: $\mathbf{q}=\mathbf{k}_1-\mathbf{k}_0$). The in-plane resolution function that results from these beam divergences is enlarged on the right. It is asymmetric because of the wide in-plane opening of detector slits. It is tangent to Eqald's sphere. The angle between the scattering vector $\mathbf{q}$ and the resolution function is the scattering angle $\theta$.

## III. DETERMINATION OF THE SURFACE MISCUT

Figure 2 shows rocking scans through some of the {110} and {310} reflections for sample 1. These reflections are forbidden in an infinite diamond structure and arise here[11] from crystal-truncation rods (CTR's),[12] which are due to the abrupt termination of the bulk substrate by the surface. The evolution of the CTR's integrated intensity with perpendicular momentum transfer $q_z$ was measured and fitted with usual models;[12] it indicated atomically smooth surfaces for the three samples.

For this study, the most important feature of the truncation rods is their splitting. Each CTR consists of two distinct peaks showing the existence of a regular array of steps, arising from a small miscut in one direction.[13] An intuitive understanding of this phenomenon, schematical-

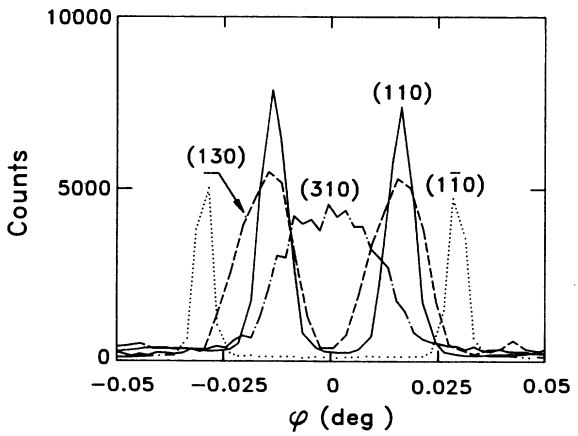


FIG. 2. Rocking scans at different in-plane truncation-rod locations of the type {110} and {310} for sample 1, as a function of the azimuthal rotation of the sample, $\phi$. Note the different peak separations as a function of the integer-order position in the reciprocal plane of the interface.

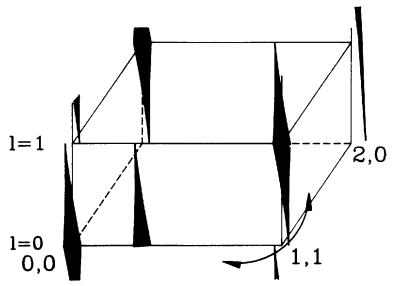


FIG. 3. Schematic representation of the reciprocal lattice of the Si(001) surface with a small miscut. The truncation rods are tilted with respect to the [001] direction of the reciprocal lattice in the direction of the miscut, by an angle equal to the miscut. At in-plane integer-order positions, two truncation rods are present, one arising from a bulk Bragg peak located below the surface reciprocal plane (defined here as the $l=0$ plane), the other arising from a Bragg peak located above the surface plane. At {110} and {310} in-plane integer-order positions, the height of the Bragg peaks producing the truncation rods measured in plane is $l=1$ RLU (RLU denotes reciprocal-lattice units), whereas it is double ($l=2$ RLU's) at {200}-type in-plane integer-order reflections.

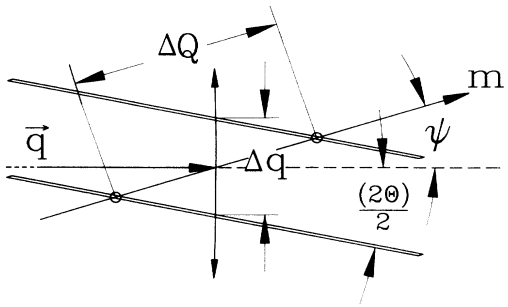


FIG. 4. Schematic representation of the way the resolution function crosses the two truncation rods (or, which is equivalent, of the way the reciprocal lattice crosses Ewald's sphere) during a rocking scan at an integer-order position. These peaks are separated by $\Delta Q$ along the miscut direction, and produce the two measured peaks separated by $\Delta q$, along the scan direction. $\psi$ is the in-plane angle between the momentum transfer, **q**, of the reflection considered and the in-plane miscut direction.

ly displayed in Fig. 3 can be achieved by considering that, since the CTR's arise from the Fourier transformation of the macroscopic truncation of the bulk lattice, they are orthogonal to the macroscopic surface (or interface), not to the crystallographic planes. This is true if the coherence length of the x-ray beam is much larger than the terrace width. Thus, the CTR's are displaced in the surface reciprocal plane from the exact integer position in the direction of the miscut $m$ by an amount of momentum transfer $\Delta Q = ml2\pi/d$ for the present case of a cubic lattice with parameter $d$, where $l$ is the height of the Bragg peak in reciprocal-lattice units (RLU's).

The measured peak separation during a rocking scan is related to both the miscut and the path of the resolution function across the two peaks in reciprocal space (Fig. 4). It is related to the true peak separation $\Delta Q$ by

$$\Delta q = \Gamma(\mathbf{q})\Delta Q \quad \text{with} \quad \Gamma(\mathbf{q}) = \left| \sin|\psi| + \cos|\psi| \tan\frac{2\theta}{2} \right| , \tag{1}$$

where $\psi$ is the angle between **q** and the in-plane miscut orientation. The values of the measured peak splitting $\Delta q$ are reported in Table II for sample 1 for most {110}, {200}, and {310} positions.

The value and in-plane orientation of the miscut, together with their uncertainties, can be determined from these measurements (see Table II). For sample 1, for instance, the miscut direction makes an angle $\psi = 16.5° \pm 1°$ with the $[1\bar{1}0]$ direction, towards the [110] direction, and the value of the miscut [that is, the angle between the macroscopic surface and the (001) atomic planes] is $m = 0.047° \pm 0.002°$. These parameters are summarized in Table I for the three samples.

Obtaining more precise information about the step arrangement requires more detailed data, such as that shown in Fig. 5 for (110) rocking-scan data from sample 1. In a quantitative analysis, one should concentrate on reproducing (i) the peak intensity ratio between the first- and second-order satellites, (ii) the small width of the two main peaks, and (iii) the shape of the diffuse component. Such an analysis will be described in the following sections, and it will serve to characterize the distribution of terrace widths and describe long-range correlations between successive terrace widths.

TABLE II. Measured CTR peak separations $\Delta q$ (column 4) for sample 1. $h$ and $k$ are the in-plane reciprocal indices; $l$ is the height of the Bragg reflections producing the CTRs. Column 5 contains the values of the peak separations recalculated from the determined orientation and value of the miscut. Column 6 contains the values of the miscut deduced at each position from the experimental separation, given the calculated ratio of the measured to actual separation, which is reported in the column 7.

| $h$ | $k$ | $l$ (Bragg) | $\Delta q$ ($10^{-4}$ Å$^{-1}$) (expt.) | $\Delta q$ ($10^{-4}$ Å$^{-1}$) (calc.) | Miscut (deg) | $\Delta q/\Delta Q$ |
|---|---|---|---|---|---|---|
| 1 | 1 | 1 | 8.5 | 8.6 | 0.0461 | 0.906 |
| 1 | −1 | 1 | 4.1 | 4.4 | 0.0475 | 0.460 |
| 2 | 0 | 2 | 5.0 | 4.9 | 0.0478 | 0.245 |
| 3 | 1 | 1 | 4.0 | 4.1 | 0.0466 | 0.429 |
| 1 | 3 | 1 | 10.2 | 10.1 | 0.0477 | 1.062 |
| 0 | 2 | 2 | 9.6 | 9.5 | 0.0473 | 1.005 |
| −1 | 3 | 1 | 4.7 | 4.4 | 0.0483 | 0.460 |

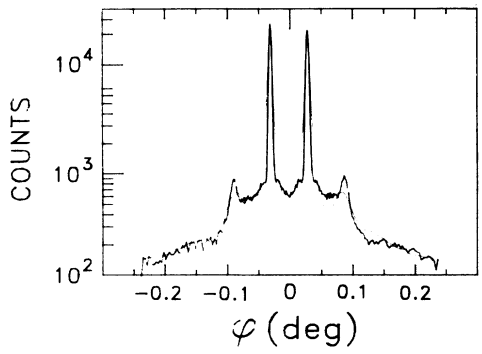


FIG. 5. Rocking scan at the {110} position for sample 1. The logarithm of the intensity is reported as a function of the azimuthal rotation $\phi$. Note the existence of second-order and even third-order reflections. Note also the characteristic shape of the diffuse component and the small width of the two main peaks. Superposed onto the experimental data (thick line) is a simulation (thin line) according to the "correlation model," with a Gaussian distribution of terrace widths. The parameters of the model are reported in Table IV. The simulations were convoluted with a Gaussian distribution of 0.003° full width at half maximum (FWHM) to account for experimental resolution. A constant background of 130 counts was added. Note that this model does not accurately reproduce the very small width of the two main peaks.

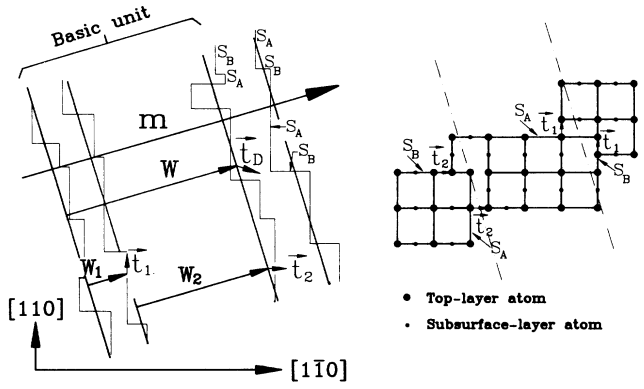


FIG. 6. Left: Schematic representation of the biterrace constituting the basic unit of the staircase of steps. **a** is a vector in the direction of the miscut, whose length is equal to the length of the surface lattice vectors $\frac{1}{2}[110]$ and $\frac{1}{2}[1\bar{1}0]$; that is, 3.84 Å. $\mathbf{W}=\Gamma(\mathbf{q})M\mathbf{a}$ is the width of the whole unit, and $\mathbf{W}_1=\Gamma(\mathbf{q})M_1\mathbf{a}$ and $\mathbf{W}_2=\Gamma(\mathbf{q})M_2\mathbf{a}$ are the widths of the two subterraces. $\mathbf{t}_1=\frac{1}{4}[11\bar{1}]$ and $\mathbf{t}_2=\frac{1}{4}[1\,\bar{1}\,\bar{1}]$ are the lattice translations that occur when crossing the first and second types of steps, respectively. On an atomic scale, steps are made of portions along the [110] direction, and portions along the $[1\bar{1}0]$ direction, of the $S_A$ or $S_B$ types according to Chadi's notation (Ref. 1). These portions are separated by kinks. The resulting step-edge roughness has been strongly exaggerated on the drawing for clarity. Right: Schematic representation of the two kinds of steps considered, with different noninteger translations $\mathbf{t}_1$ and $\mathbf{t}_2$, both around a kink, so that both kinds of substeps, of $S_A$ and $S_B$ types, are shown.

## IV. DIFFRACTION MEASUREMENT OF STAIRCASES OF STEPS

### A. Introduction

A suitable calculation of the measured CTR intensity distributions must include the discrete nature of the lattice underlying the miscut surface. This miscut supposedly arises from an array of nearly regularly spaced steps whose edges are nearly straight and orthogonal to the in-plane miscut orientation (Fig. 6). On the Si(001) surface, crossing a monolayer-high step results in both in-plane and out-of-plane translations, plus a 90° rotation of the lattice with respect to the [110] direction, which are responsible for a phase shift between the wave scattered by the upper terrace and the wave scattered by the lower terrace. Depending on the value of the momentum transfer **q**, two successive terraces may scatter constructively, destructively, or with any intermediate phase shift. For in-plane scattering ($q_z \approx 0$), only the in-plane components of the translations participate to the phase shift. Two kinds of alternating monolayer-high steps have to be considered, with two different in-plane translations: $\mathbf{t}_1=\frac{1}{4}[11]$ and $\mathbf{t}_2=\frac{1}{4}[1\bar{1}]$. For the present in-plane scattering configuration, the surface thus consists of a staircase of basic units made of two adjacent terraces, with an additional phase shift $\mathbf{q}\cdot\mathbf{t}_D$ introduced between successive units, where $\mathbf{t}_D=\mathbf{t}_1+\mathbf{t}_2$. An atom on a given terrace is related to an atom on a successive terrace by a translation $\mathbf{T}=\mathbf{t}_{\rm lat}+\mathbf{t}$, where $\mathbf{t}_{\rm lat}$ is a translation of the bulk silicon lattice, and **t** (either $\mathbf{t}_1$ or $\mathbf{t}_2$ or $\mathbf{t}_D$) is a noninteger translation.

### B. Reduction to one dimension

This problem can be greatly simplified by reducing the analysis to one dimension. At first, consider only two adjacent terraces. Let us define a reciprocal-lattice vector $\mathbf{b}_m$ along the miscut direction. Using $\mathbf{b}_m$, the intensity can be calculated as if the momentum-transfer variation was along the miscut direction, instead of the actual direction transverse to **Q** (the momentum transfer corresponding to the exact integer-order position). The momentum transfer **q** can be written as

$$\mathbf{q}=\mathbf{Q}+2\pi h_m\mathbf{b}_m\Gamma(\mathbf{q})=\mathbf{Q}+2\pi h\mathbf{b}_m \quad \text{with } h=h_m\Gamma(\mathbf{q}) , \tag{2}$$

where $h_m$ is the reciprocal-lattice-unit variation along the miscut direction. The phase shift can now be rewritten as

$$\begin{aligned}\mathbf{q}\cdot\mathbf{T}&=(\mathbf{Q}+2\pi h\mathbf{b}_m)\cdot(\mathbf{t}_{\rm lat}+\mathbf{t})\\&=\mathbf{Q}\cdot\mathbf{t}_{\rm lat}+\mathbf{Q}\cdot\mathbf{t}+2\pi h\mathbf{b}_m\cdot\mathbf{t}_{\rm lat}+2\pi h\mathbf{b}_m\cdot\mathbf{t} .\end{aligned} \tag{3}$$

Since $h$ is always small, the last term can be neglected. The first term is a multiple of $2\pi$, and can thus be omitted. The second term has a value of either 0 or $\pi$. The phase-shift variation along the scan direction is thus contained in the third term. Now consider a one-dimensional staircase of point scatterers made of lines of atoms separated by steps, such that, within a line, the lattice parameter is $a=2\pi/b_m=3.84$ Å, and such that

steps introduce a phase shift of $\mathbf{Q}\cdot\mathbf{t}$. Let $h$ be the reduced reciprocal-lattice unit along the direction of the lines. The lattice component, $\mathbf{t}_{\text{lat}}$, of the translation between two lines can be expressed as a multiple of the lattice parameter $a$ by $\mathbf{t}_{\text{lat}}=Ma$. The phase shift between two lines will have the above form, where the third term can be expressed as a function of $M$ by

$$2\pi h\mathbf{b}_m\cdot\mathbf{t}_{\text{lat}}=2\pi hM \ . \tag{4}$$

This shows that the problem is analogous to a staircase of point scatterers along a line parallel to the miscut direction, with lattice parameter $a$ in this direction, but with translations between successive terraces arising from the three-dimensional nature of the problem. The lines of atoms of this model will be called terraces, and the values $M$ will be called number of unit cells in a terrace, although this does not have a direct meaning for the two-dimensional case of interest. The true terrace width $W$ is related to the calculated one by $W=\Gamma(\mathbf{q})Ma$. For simplicity, the $\Gamma(\mathbf{q})$ scaling factor will often be omitted in the following calculations.

To describe the one-dimensional staircase, an origin is arbitrarily defined at the beginning of one unit, which allows us to assign a subscript $l$ to a particular unit. The unit $l$ is made of two terraces of respective length $M_{1l}a$ and $M_{2l}a$, separated by steps yielding respective phase shifts of $\mathbf{Q}\cdot\mathbf{t}_1$ and $\mathbf{Q}\cdot\mathbf{t}_2$; its origin is defined by the vector $\mathbf{R}_l$.

### C. Calculation of the diffraction

In general, there are two possible approaches to calculate the diffraction from a given assembly of atoms: the correlation-function approach and the direct approach.[14] Each has its specific advantages and drawbacks; both will be considered.

In the direct-calculation approach, the diffracted intensity is developed as the statistical average of the square of the scattering amplitude $S(\mathbf{q})$:

$$I(\mathbf{q})=C\langle S(\mathbf{q})S^*(\mathbf{q})\rangle \ , \quad S(\mathbf{q})=f(\mathbf{q})\sum\exp(i\mathbf{q}\cdot\mathbf{r}) \ , \tag{5}$$

where $C$ is a constant; $f(\mathbf{q})=g(\mathbf{q})C_{\text{CTR}}(\mathbf{q})$, where $g(\mathbf{q})$ is the scattering factor from a row of atoms parallel to the step edges' mean direction, and $C_{\text{CTR}}(\mathbf{q})$ is the contribution from a column of atoms, in the direction normal to the terraces ([001]).[12] $f(\mathbf{q})$ is the scattering factor of the corresponding plane of atoms. $\mathbf{r}$ represents at atomic position in the terrace, in the direction of the miscut. We assume in the following that the step edges are perfectly straight, i.e., that no kinks are involved. Although this assumption may seem unrealistic for a general in-plane orientation of the miscut, since elementary steps are either along [110] or along $[1\bar{1}0]$, we will show that the detailed structure of step edges is negligible in the present case. Accordingly, the scattered amplitude is given by

$$S(\mathbf{q})=f(\mathbf{q})\sum_{l=-\infty}^{0}\exp(i\mathbf{q}\cdot\mathbf{R}_l)\left[\sum_{p=0}^{M_{2l}-1}\exp(i\mathbf{q}\cdot\mathbf{a}p)+\exp(i\mathbf{q}\cdot\mathbf{R}_{2l})\sum_{r=0}^{M_{1l}-1}\exp(i\mathbf{q}\cdot\mathbf{a}r)\right]$$
$$+f(\mathbf{q})\sum_{l=1}^{+\infty}\exp(i\mathbf{q}\cdot\mathbf{R}_l)\left[\sum_{p=0}^{M_{1l}-1}\exp(i\mathbf{q}\cdot\mathbf{a}p)+\exp(i\mathbf{q}\cdot\mathbf{R}_{1l})\sum_{r=0}^{M_{2l}-1}\exp(i\mathbf{q}\cdot\mathbf{a}r)\right]$$

$$\text{where } \mathbf{R}_{1l}=M_{1l}\mathbf{a}+\mathbf{t}_1 \ , \quad \mathbf{R}_{2l}=M_{2l}\mathbf{a}+\mathbf{t}_2 \ , \quad \mathbf{R}_l=\sum_{p=0}^{l-1}(M_p\mathbf{a}+\mathbf{t}_D) \ .$$

$M_p=M_{1p}+M_{2p}$ is the total number of unit cells in the $p$ unit.

For a perfectly regular array of $N$ ($N\to\infty$) units, $M_{1l}=M_1$, $M_{2l}=M_2$, and $M_l=M_1+M_2=M$ are constant; the diffracted intensity is simply given by

$$I\propto\frac{\sin^2[(\pi M h+\mathbf{Q}\cdot\mathbf{t}_D)N]}{\sin^2[\pi Mh+\mathbf{Q}\cdot\mathbf{t}_D]}\,\frac{\sin^2(\pi hM_1)+\sin^2(\pi hM_2)+2\sin(\pi hM_1)\sin(\pi hM_2)[\cos(\pi Mh+\mathbf{Q}\cdot\mathbf{t}_1)+\cos(\pi Mh+\mathbf{Q}\cdot\mathbf{t}_2)]}{\sin^2\pi h} \ , \tag{6}$$

where $h$ is such that $\mathbf{q}\cdot\mathbf{a}=2\pi n+2\pi h$, where $n$ is an integer. The second term of the above expression describes the diffraction within the basic unit, and the first one the diffraction from the grating. The peak separation $(1/M)$ yields the whole unit width:

$$W=Ma\Gamma(\mathbf{q}) \ . \tag{7}$$

In practice, this width is more precisely determined from the miscut value, $m$, and the height different introduced by a unit (that is, $d=a_z/2$, where $a_z=5.431$ Å is the silicon lattice parameter) by $W=d/m$. The average biterrace unit widths thus determined are reported in Table I for the three samples.

Table III summarizes the values taken by the three phase shifts $\mathbf{Q}\cdot\mathbf{t}_D$, $\mathbf{Q}\cdot\mathbf{t}_1$, and $\mathbf{Q}\cdot\mathbf{t}_2$, at the different in-plane integer-order positions where the CTR's intensities were measured. At the exact integer-order position ($h=0$), the successive units scatter out of phase and the two subterraces scatter in phase for $\mathbf{Q}=\{110\}$ and $\mathbf{Q}=\{310\}$, whereas the biterrace units scatter in phase but the two subterraces of a unit scatter out of phase for $\mathbf{Q}=\{200\}$. Figure 7 shows the intensity dependence on the value of

TABLE III. Values of the three phase shifts, $\mathbf{Q}\cdot\mathbf{t}_1$, $\mathbf{Q}\cdot\mathbf{t}_2$, and $\mathbf{Q}\cdot\mathbf{t}_D$, at {110} and {200} exact in-plane integer-order positions.

| Q | (110) | $(1\bar{1}0)$ | (310) | $(3\bar{1}0)$ | (200) | (020) |
|---|---|---|---|---|---|---|
| $\mathbf{Q}\cdot\mathbf{t}_1$ | $\pi$ | 0 | 0 | $\pi$ | $\pi$ | $\pi$ |
| $\mathbf{Q}\cdot\mathbf{t}_2$ | 0 | $\pi$ | $\pi$ | 0 | $\pi$ | $\pi$ |
| $\mathbf{Q}\cdot\mathbf{t}_D$ | $\pi$ | $\pi$ | $\pi$ | $\pi$ | 0 | 0 |

Q and the ratio between $M_1$ and $M_2$, for this ideal case of perfect order. The intensity distribution at the {110} and {310} positions depends little on the ratio $M_1/M_2$; on the other hand, at {200}, varying this ratio strongly affects the intensity. When $M_1=M_2$, the intensity is minimum at the exact {200} position. When $M_1=0$ (i.e., only one type of terrace exists) the amplitudes add at the exact {200} positions (note that the intuitive explanation fails for this case). When the ratio $M_1/M_2$ is varied, the proportion of the terraces that interfere destructively and constructively varies, and the intensity distribution is intermediate. Thus, {200} data are significantly affected by the unit structure, and the disorder of both kinds of subterraces should be accounted for to simulate these data. By contrast, {110} and {310} data mainly contain information on the repartition of the whole biterrace units.

As shown in Appendix A, since the {110} and {310} data are nearly insensitive to the precise biterrace unit configuration, these data can be simulated by assuming a single terrace whose interterrace translation is $\mathbf{t}_D$. This approach cannot be used to simulate {200} data, since the disorder within the unit is important for those reflections. Considering an array of uniform terraces separated by fictitious bilayer high steps, we introduce the deviation $m_l$ from the mean value $M$ of the number of unit cells in the $l$ terrace:

$$M_l=M+m_l \quad \text{with } \langle m_l\rangle=0 \; . \tag{8}$$

As shown in Appendix B, all the intensity can be expressed, within the small-disorder approximation, as a function of the mean number $M$, the root-mean-square (rms) variation of the terrace width $\sigma=(\langle m_p^2\rangle)^{1/2}$, and the correlation parameter between two terraces $p$ and $q$ ($p\neq q$): $\langle m_p m_q\rangle$. Hence, the direct calculation allows us to account for the correlations $\langle m_p m_q\rangle$. Nevertheless, the small-disorder approximation may not always be valid, in which case one has to use a model of the terrace-width distribution, and thus refer to the "correlation-function models."

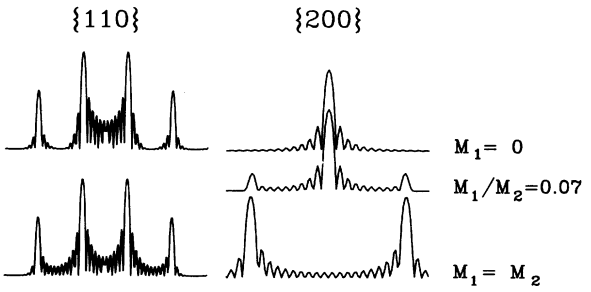


FIG. 7. Calculated intensity for a perfectly ordered staircase of biterrace units, around {110} and {200} in-plane integer-order positions, for different ratios of the two subterrace widths $\Gamma(\mathbf{q})aM_1$ and $\Gamma(\mathbf{q})aM_2$. The logarithm of the intensity is shown as a function of the reduced coordinate $h$ (arbitrary units).

In the correlation-function approach, a specific form of the correlation function (the probability that two steps are separated by a given vector) has to be assumed.[15] The most comprehensive model (referred to as the PLC model in the following, after Pukite, Lent, and Cohen[16]) assumes statistical independence between neighboring terrace widths: the probability of finding a terrace of a certain width, displaced by a certain amount from a neighboring terrace, is independent of the neighbor's width; i.e., there are no correlations between terrace widths. Another limitation is that only a single type of defect is considered; therefore, again, this model cannot be used to describe the {200} data, but is well suited to simulate {110} and {310} data. We refer to the original paper[16] for the derivation of the intensity where the step height D has to be replaced by the total translation $\mathbf{t}_D$.

## V. SIMULATION OF THE EXPERIMENTAL DATA

The analysis will be performed in two steps. First, the {200} data will be used to estimate, from the direct calculation for a perfectly ordered array, the mean configuration of the unit; that is, the average ratio of the two subterraces' widths. In the second step, the {110} data will be simulated by replacing the biterrace unit by only one terrace.

Figure 8 shows the experimental data for the {200} transverse scans of samples 1 and 2, respectively. These two scans differ markedly: for sample 1, there is a strong central peak with weak satellites, showing that one subterrace is narrow. By comparing the experimental respective intensities of these central and off-centered

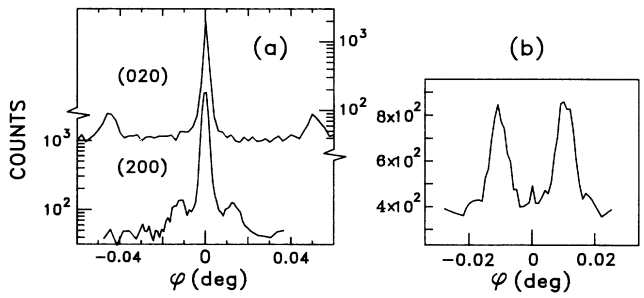


FIG. 8. (a) {200} transverse-scan data for sample 1. The logarithm of the intensity is reported as a function of the azimuthal sample-rotation angle $\phi$. In addition to a strong central component, weaker satellites are present. Their relative magnitudes yield an estimate of the ratio of the two subterrace widths: $M_1/M_2\sim 0.07$ (see Fig. 7). (b) {200} transverse-scan data for sample 2. In contrast to sample 1, the central component is weak, and two strong satellites are present. This shows that the two subterraces have equal mean width: $M_1\sim M_2$.

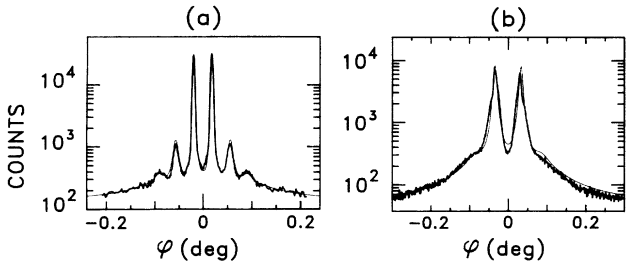


FIG. 9. {110} transverse-scan data for (a) sample 2 and (b) sample 3. The logarithm of the intensity is reported as a function of the azimuthal angle $\phi$. Superposed on the experimental data (thick lines) are simulations (thin lines) according to the "correlation model" (Ref. 16), with a Gaussian distribution of terrace widths. The parameters of the model are reported in Table IV. The simulations were convoluted with a Gaussian distribution of 0.003° FWHM to account for experimental resolution, and constant backgrounds of (a) 100 counts and (b) 60 counts, respectively, were added.

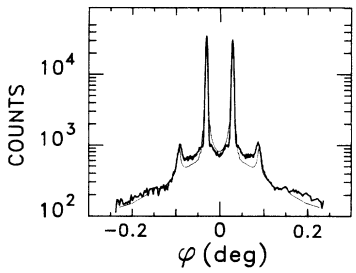


FIG. 10. {110} transverse scans data for sample 1. The logarithm of the intensity is reported as a function of the azimuthal angle $\phi$. Superposed on the experimental data (thick line) is a simulation (thin lines) according to the "direct" model, within the small-disorder approximation, and with long-range terrace-width correlations, as described in the text. The parameters of the model are reported in Table IV. The simulations were not convoluted, but instead, a limited number of coherently diffracting steps was considered to account for experimental resolution. A constant background of 120 counts was added. The small width of the main two peaks is now well reproduced, in contrast to previous simulations (Fig. 5), where terrace widths were supposed to be uncorrelated.

peaks to the calculated ones (see Fig. 7), the ratio $M_1/M_2$ is found to be $\sim 0.07$. This ratio is a rough estimate because disorder has been ignored in the calculation. Since the miscut determination yielded a whole unit width of $W=\Gamma(\mathbf{q})Ma=3300$ Å, the mean widths of the two subterraces can be deduced from this ratio: $W_1=\Gamma(\mathbf{q})M_1a\sim 240$ Å and $W_2=\Gamma(\mathbf{q})M_2a\sim 3060$ Å. Sample 2 has a small central contribution and most of the intensity is in the satellites. This is clearly a case where the two subterraces are of equal width ($W_1 \sim W_2 \sim 2500$ Å). The small central peak presumably arises from a small amount of disorder within the biterrace unit.

Because of its simplicity, the "correlation-function" model described above was first used to simulate the {110} data. Figures 5 and 9 show the best simulations of the {110} data obtained with this model for the three samples while employing a Gaussian distribution of terrace widths. Table IV contains the corresponding values of the rms width variation $\sigma$. For samples 2 and 3, the experimental intensity distribution is well accounted for by this model. By contrast, for sample 1, calculated peaks are much wider than experimental ones. This discrepancy in peak widths can be explained by including long-range correlations between successive terrace widths, using the "direct approach" and the small-disorder approximation. The functional form chosen for the correlations is based on the constraint that the overall miscut remains constant. This requires that if one terrace is wider than the average, the neighboring terraces are narrower, but with decreasing amplitude. An exponential function of the form

$$\langle m_p m_q \rangle = -\alpha^2 \exp[-|(p-q)|/P] \tag{9}$$

was chosen for its simplicity and since it yields a characteristic length $PMa\Gamma(\mathbf{q})$ over which the correlations extend (where $P$ is the corresponding characteristic number of terraces). Figure 10 shows the best simulations of the (110) truncation-rod data of sample 1 obtained with this

TABLE IV. Values of the different parameters used for the simulations of the (110) truncation rods for the three samples. Simulations according to the model of Pukite *et al.* (Ref. 16) are denoted by PLC, by contrast with "direct" simulations. Column 4 contains the parameter $M$, the number of unit cells in a basic unit, in the one-dimensional analogue to the present two-dimensional problem. Column 5 contains the biterrace unit width deduced from the parameter $M$. Column 6 contains the rms unit-width variation given in unit cells for the one-dimensional analogue, and column 7 contains the rms unit-width variation after rescaling. Columns 8–10 contain the $\alpha$ and $P$ parameters, describing the terrace-width correlations, and the number $N$ of units scattering coherently within the coherence length of the x-ray beam for the "direct model."

| Sample No. | (*hkl*) | Model | $M$ | $\Gamma(\mathbf{q})Ma$ (Å) | $\sigma$ | $\Gamma(\mathbf{q})\sigma a$ (Å) | $\alpha$ | $P$ | $N$ |
|---|---|---|---|---|---|---|---|---|---|
| 1 | (110) | PLC | 940 | 3300 | 200 | 700 | | | |
| | (110) | direct | 940 | 3300 | 120 | 420 | 35 | 12 | 10 |
| 2 | (110) | PLC | 1500 | 4800 | 220 | 1050 | | | |
| 3 | (110) | PLC | 900 | 2300 | 350 | 900 | | | |

direct model. In these simulations, the effect of experimental resolution is included by considering only a finite number of terraces. This simulation accurately reproduces the experimental features including the respective intensities of the first- and second-order peaks, and the narrow central peaks. The actual peak width corresponds to a correlation length of $P \sim 12$ steps, with a correlation parameter $\alpha = 35$ units cells in the miscut direction. This correlation is large by comparison to the maximum allowed value $\alpha_{\max} = \sigma/2 = 60$. The widths of the two main peaks are resolution limited and are not critically sensitive to variations of $P$ from 9 to 15. Thus, the value of $\Gamma(\mathbf{q})PMa \sim 4$ $\mu$m is a lower bound and may be greater than the coherence length of the x-ray beam for this reflection of $\sim 4.6$ $\mu$m. The parameter $\alpha$ is correlated to the length $P$ and the number of diffracting steps in the irradiated area, $N$, so that its value is not precisely meaningful; it only suggests the existence of strong terrace-width correlations extending over several micrometers.

## VI. DISCUSSION

We now discuss and compare the analysis of the intensity distribution for the three samples. On sample 3, the (110) data (Fig. 9) are made up of only two peaks, much wider than those of the first samples. The unit-width disorder is thus large: simulations yield $\Gamma(\mathbf{q})a\sigma_{(110)} \sim 900$ Å (that is, 35% of the mean terrace width of 2600 Å). On this sample, the disorder is too large for the "small-disorder" approximation to be valid, so that one must resort to models that neglect terrace-width correlations. The large step disorder can be attributed either to the lack of a high-temperature anneal, or to roughening during the 1-week-long oxidation at room temperature. We expect the former effect to be dominant, since significant roughening is not expected for native oxidation at room temperature for such a short duration.

For sample 2, which was shown to have a nearly regular array of monolayer-high steps, three orders of diffraction were present. The experimental intensity distribution is accurately reproduced by simulations with the "correlation-function" model. The rms unit-width variations deduced from simulations are $\Gamma(\mathbf{q})a\sigma_{(110)} \sim 700$ Å (14% of the mean terrace width of 5000 Å).

For sample 1, surprisingly, {200} data show that within the unit, one subterrace is much wider than the other. Although this could be explained if the sample has been analyzed after abruptly stopping the MBE step-flow process, it is not expected for an unstrained sample annealed at high temperature. One possible explanation is that the sample was under stress during the high-temperature annealing, or during the subsequent cooling down to room temperature. In that case, a recent STM study showed that the ratio of the two subterrace widths could be drastically affected.[17] However, the sample mounting was designed to minimize such stresses and was identical for all the samples studied here.

The present data are not precise enough to deduce the exact form of these long-range correlations between successive terrace widths. Several different functions were used to model these correlations and simulate our data. Assuming the proper parameters, they did not yield significantly different results. However, the requirement to introduce the correlations in our model was clear and their amplitude and lateral range were model independent. Thus, the present study proves the existence of correlations, but yields only estimates of their magnitude and extension. When neglecting these correlations, the rms disorder deduced from simulations [$\Gamma(\mathbf{q})a\sigma_{(110)} \sim 700$ Å; that is, 21% of the mean terrace width of 3300 Å] is larger than when correlations are introduced [$\Gamma(\mathbf{q})a\sigma_{(110)} \sim 420$ Å; that is, 13% of the mean terrace width]. The step disorder is similar to that on sample 2, which may be attributed to nearly identical preparation conditions, except for possible additional stress on sample 1.

It is important to note that the meaning of the rms disorder is not as straightforward as supposed in the model. We have assumed that the edges are straight, or, in other words, that the edge roughness is included in the terrace-width disorder measured here. The disorder actually arises from two contributions. The first contribution is the terrace-width distribution around the mean terrace width $M$; the second contribution is from the step roughness.[15] In the present experiment, the angles between the incident or exit beams and the step edges' mean direction are neither 0 nor $\pi/2$, but instead vary with the particular reflection considered, so that both kinds of disorder are actually measured, with different proportions according to the azimuthal angle.

## VII. CONCLUSIONS

Grazing-incidence x-ray scattering proves to be a powerful tool with which to study step topography at surfaces and interfaces, and, in particular, to analyze the step arrangement and terrace-width distribution on miscut surfaces. It provides information complementary to that gained by other techniques such as ARLS, low-energy electron diffraction, or STM. Because of the very good resolution of the experiment, the diffraction features obtained are much more sharply defined than with other techniques. This resolution is critical since it enables us to show the existence, in some cases, of long-range correlations between the widths of successive terraces, which are responsible for the preservation of the regular staircase over long distances, despite the large distribution of individual terrace widths.

Three samples of the Si(001)/$SiO_2$ interface were studied, with different amounts of step disorder. On all samples, the regular staircase of steps was preserved during the oxidation process. The small miscut values, $\sim 0.05°$, and in-plane orientation have been determined with a high accuracy. Analyses of the in-plane truncation-rod data were done assuming diffraction by a disordered staircase of basic units made of two subterraces separated by inequivalent steps. {200} data yielded an estimate of the ratio of the two subterrace widths, while simulation of {110} truncation-rod data yielded the mean unit width and the root-mean-square unit-width disorder.

The sample that was not annealed at high temperature and whose oxidation duration was longer than the others

displayed the more disordered steps, with a rms width disorder ~30% of the mean terrace width. On the two other samples, which were annealed at high temperature after MBE deposition, and oxidized for a short time, the terrace width disorder was smaller: ~15% of the mean terrace width. On one of these, the basic unit was symmetric, as expected, while on the other, one subterrace was narrow (~240 Å) and the other wide (~3060 Å). In addition to this difference between the two samples, long-range correlations between terrace widths, extending over several micrometers, were shown to exist on the second sample, but not on the first. A possible explanation for these differences is that the second sample was under stress during the preparation process.

## ACKNOWLEDGMENTS

These experiments were performed on the AT&T Bell Laboratories X16A beam line at the National Synchrotron Light Source of Brookhaven National Laboratory, which is supported by the U.S. Department of Energy. We acknowledge valuable discussions with A. Bourret, K. Evans-Lutterodt, A. Ourmazd, I. K. Robinson, and E. Vlieg. We thank P. O. Hahn for providing the substrates used for these experiments.

## APPENDIX A

In this appendix the implications of the approximation carried out by replacing the biterrace unit with a unique terrace are discussed. Two cases will be encountered in this study. The first occurs when the width of one terrace is negligible with respect to the second (which is the case of sample 1, as will be shown). In that case, the approximation consists of neglecting the small interference between the first terrace and a band of equal width of the second terrace. The second case occurs when the mean widths of the two subterraces are equal (which is the case of sample 2). In that case, we further suppose that for each biterrace unit $l$, the two subterraces have equal widths $M_{1l}=M_{2l}=M_l/2$. The amplitude scattered by the array of biterraces is then given by

$$S(\mathbf{q})=f(\mathbf{q})\sum_{l=0}^{+\infty}\exp(i\mathbf{q}\cdot\mathbf{R}_l)\sum_{p=0}^{M_l/2-1}\exp(i\mathbf{q}\cdot\mathbf{a}p)\left\{2+\exp\left[i\mathbf{q}\cdot\left[\frac{M_l}{2}\mathbf{a}+\mathbf{t}_2\right]\right]+\exp\left[i\mathbf{q}\cdot\left[\frac{M_l}{2}\mathbf{a}+\mathbf{t}_1\right]\right]\right\}. \tag{A1}$$

We restrict this analysis to {110} or {310} data, where either $\mathbf{q}\cdot\mathbf{t}_1$ or $\mathbf{q}\cdot\mathbf{t}_2$ is a multiple of $\pi$ and the other is a multiple of $2\pi$, so that the terms containing $\mathbf{t}_1$ and $\mathbf{t}_2$ cancel out. The scattered amplitude simplifies to

$$S(\mathbf{q})=2f(\mathbf{q})\sum_{l=0}^{+\infty}\exp(i\mathbf{q}\cdot\mathbf{R}_l)\sum_{p=0}^{M_l/2-1}\exp(i\mathbf{q}\cdot\mathbf{a}p)\,. \tag{A2}$$

Comparing this expression with that of $S(\mathbf{q})$ for an array of bilayer-high steps separated by the whole unit width, we see that the difference is in the last summation, up to $M_l/2-1$ in one case,and $M_l-1$ in the other. A simple calculation (or application in the case of perfect order) of these two intensity expressions as a function of $h$ shows that they are nearly identical, after scaling the former by a factor of 2, except for diffuse components which are more than three orders of magnitude weaker than the main peaks, and hence one order of magnitude weaker than the experimental background.

## APPENDIX B

In this appendix the main steps of the derivation of the intensity scattered by the disordered staircase of steps within the small-disorder approximation are summarized, assuming a single type of (bilayer high) steps. Let us define

$$\mathbf{R}_l=\sum_{i=0}^{i=l-1}M_i\mathbf{a}+l\mathbf{t}_D=l\mathbf{R}+n_l\mathbf{a}\quad\text{where }\mathbf{R}=M\mathbf{a}+\mathbf{t}_D\quad\text{and }n_l=\sum_{i=0}^{i=l-1}m_i\,. \tag{B1}$$

$n_l\mathbf{a}$ is the length variation of $\mathbf{R}_l$ with respect to its average value of $l\mathbf{R}$. By definition, $\langle n_l\rangle=0$. For $N$ diffracting steps, the scattered amplitude can be rewritten as

$$S(\mathbf{q})=\sum_{p=0}^{N-1}\exp(i\mathbf{q}\cdot\mathbf{R}_p)\sum_{s=0}^{M_p-1}f(\mathbf{q})\exp(i\mathbf{q}\cdot\mathbf{a}s)\,. \tag{B2}$$

A straightforward calculation of the square of this expression leads to

$$S(\mathbf{q})S^*(\mathbf{q})=f^2(\mathbf{q})\sum_{p=-}^{N-1}\sum_{r=0}^{N-1}\exp[1/2i\mathbf{q}\cdot\mathbf{a}(m_p-m_r)]\exp[i\mathbf{q}\cdot\mathbf{a}(n_p-n_r)]\exp[i(p-r)\mathbf{q}\cdot\mathbf{R}]B_{p,r}(\mathbf{q})\,, \tag{B3}$$

where

$$B_{p,r}(\mathbf{q})=\sin[1/2(M+m_p)\mathbf{q}\cdot\mathbf{a}]\sin[1/2(M+m_1)\mathbf{q}\cdot\mathbf{a}]\frac{1}{\sin^2(1/2\mathbf{q}\cdot\mathbf{a})}\,. \tag{B4}$$

$B_{p,r}(\mathbf{q})$ can be developed in second order with respect to $m_p\mathbf{q}\cdot\mathbf{a}$ and $m_r\mathbf{q}\cdot\mathbf{a}$, in the approximation of small terrace-width disorder ($m_p 2\pi h \ll 1$ and $m_r 2\pi h \ll 1$):

$$B_{p,r}(\mathbf{q}) \approx \beta \sin^2(1/2M\mathbf{q}\cdot\mathbf{a}) + 1/2\beta\mathbf{q}\cdot\mathbf{a}(m_p+m_r)\sin(1/2M\mathbf{q}\cdot\mathbf{a})\cos(1/2M\mathbf{q}\cdot\mathbf{a}) + 1/4\beta m_p m_r(\mathbf{q}\cdot\mathbf{a})^2\cos(1/2M\mathbf{q}\cdot\mathbf{a}) , \quad \text{(B5)}$$

where

$$\beta = \frac{1}{\sin^2(1/2\mathbf{q}\cdot\mathbf{a})} .$$

At this point, one should calculate the statistical average:

$$\langle \exp[1/2i\mathbf{q}\cdot\mathbf{a}(m_p - m_r + 2n_p - 2n_r)] B_{p,r}(\mathbf{q}) \rangle . \quad \text{(B6)}$$

By developing the exponential and keeping only the second-order terms in $m_p\mathbf{q}\cdot\mathbf{a}$, one finds, with the additional assumption that $2\pi h(m_p - m_r + 2n_p - 2n_r) \ll 1$,

$$\exp\left[-\frac{(\mathbf{q}\cdot\mathbf{a})^2}{8}\langle (m_p - m_r + 2n_p - 2n_r)^2 \rangle\right] \sin^2(1/2M\mathbf{q}\cdot\mathbf{a}) + \tfrac{1}{4}\langle m_p m_r \exp[i\mathbf{q}\cdot\mathbf{a}(m_p - m_q) + 2n_p - 2n_q] \rangle \times (\mathbf{q}\cdot\mathbf{a})^2 \cos^2(1/2M\mathbf{q}\cdot\mathbf{a}) . \quad \text{(B7)}$$

Note that the above assumption can only be realized for small $h$ values, or if strong (negative) correlations are introduced, so that the $n_p$ parameters are of order the $m_p$ ones. The first statistical average can be easily calculated as a function of the terrace-width correlation and rms disorder parameters according to

$$\text{(B8)} \quad \langle n_p n_q \rangle = \sum_{k=0}^{i=p-1} \sum_{j=0}^{j=q-1} \langle m_i m_j \rangle$$

and

$$\langle m_p n_q \rangle = \sum_{k=0}^{i=q-1} \langle m_p m_i \rangle .$$

The second statistical average to calculate is

$$\langle m_p m_q \exp(1/2i\mathbf{q}\cdot\mathbf{a})(m_p - m_q + 2n_p - 2n_q) \rangle . \quad \text{(B9)}$$

If $p = q$, one finds $\sigma^2$. If $p \neq q$, the calculation of this term requires further assumptions relative to higher-order correlations; we have chosen to represent the damping term by a Debye-Waller-like term of the form

$$\langle m_p m_q \rangle \exp[-(\mathbf{q}\cdot\mathbf{a})^2\gamma^2] . \quad \text{(B10)}$$

We found that this is not the exact form of the damping for this diffuse term, but is acceptable for the center of the spectrum. $\gamma$ was used in the simulations as a variable parameter. It turned out to be close to the rms length variation $\sigma$, and, accordingly, was fixed to this parameter $\sigma$, thus avoiding an additional parameter. After whole development, the intensity was expressed as a function of the reciprocal-lattice-unit coordinate along the miscut direction, $h$, the number of steps, $N$, the mean unit width, $M$, the root-mean-square variation of the terrace width, $\sigma = (\langle m_p^2 \rangle)^{1/2}$, the phase shifts $\mathbf{q}\cdot\mathbf{t}_1$, $\mathbf{q}\cdot\mathbf{t}_2$, and $\mathbf{q}\cdot\mathbf{t}_D$, and the correlation parameters between two steps $p$ and $q$ ($p \neq q$), $\langle m_p m_q \rangle$.

*Present address: Centre Etudes Nucleaires, Boîte Postale 85X, 38041 Grenoble, France.

[1]D. J. Chadi, Phys. Rev. Lett. **59**, 1691 (1987); W. Weiss, D. Schmeisser, and W. Gopel, *ibid.* **60**, 1326 (1988).
[2]Y. W. Mo, B. S. Swartzentruber, R. Kariotis, M. B. Webb, and M. G. Lagally, Phys. Rev. Lett. **63**, 2393 (1989); D. Srivastava, B. Garrison, and D. W. Brenner, *ibid.* **63**, 302 (1989).
[3]A. J. Hoeven, J. M. Lenssinck, D. Dijkkamp, E. J. Loenen, and J. Dieleman, Phys. Rev. Lett. **63**, 1830 (1989).
[4]P. E. Wierenga, J. A. Kubby, and J. E. Griffith, Phys. Rev. Lett. **59**, 2169 (1987).
[5]T. Sakamoto and G. Hashiguchi, Jpn. J. Appl. Phys. (Pt. 2) **25**, L78 (1986); T. Doi and M. Ichikawa, J. Cryst. Growth **95**, 468 (1989); T. Sakamoto, T. Kawamura, S. Nago, G. Hashiguchi, S. Sakamoto, and K. Kuniyoshi, *ibid.* **81**, 59 (1987).
[6]T. Nakayama, Y. Tanishiro, and K. Takayanagi, Jpn. J. Appl. Phys. (Pt. 2) **26**, L280 (1987).
[7]P. O. Hahn, M. Grunder, A. Schnegg, and H. Jacob, Appl. Surf. Sci. **39**, 436 (1989).
[8]B. W. Holland, C. B. Duke, and A. Paton, Surf. Sci. **140**, L269 (1984); W. S. Yang, F. Jona, and P. M. Marcus, Phys. Rev. B **28**, 2049 (1983).
[9]P. H. Fuoss and S. Brennan, Annu. Rev. Mater. Sci. **20**, 365 (1990); I. K. Robinson, in *Handbook on Synchrotron Radiation, Vol III,* edited by D. E. Moncton and G. S. Brown (Elsevier, New York, 1991).
[10]P. H. Fuoss and I. K. Robinson, Nucl. Instrum. Methods A **222**, 164 (1984).
[11]G. Renaud, P. H. Fuoss, A. Ourmazd, J. Bevk, B. S. Freer, and P. O. Hahn, Appl. Phys. Lett. **58**, 10 (1991).
[12]S. R. Andrews and R. A. Cowley, J. Phys. C **18**, 6427 (1985); I. K. Robinson, Phys. Rev. B **33**, 3830 (1986).
[13]M. Henzler, Appl. Surf. Sci. **11/12**, 450 (1982); Appl. Phys. **9**, 11 (1976).
[14]J. M. Cowley, *Diffraction Physics* (North-Holland, New York, 1975).
[15]D. Saloner, J. A. Martin, M. C. Tringides, D. E. Savage, C. E. Aumann, and M. G. Lagally, J. Appl. Phys. **61**, 15 (1987).
[16]P. R. Pukite, C. S. Lent, and P. I. Cohen, Surf. Sci. **161**, 39 (1985).
[17]B. S. Swartzentruber, Y. W. Mo, M. B. Webb, and M. G. Lagally, J. Vac. Sci. Technol. A **8**, 210 (1990).